A major purpose of the Technical Information Center is to provide the broadest dissemination possible of information contained in DOE's Research and Development Reports to business, industry, the academic community, and federal, state and local governments.

Although a small portion of this report is not reproducible, it is being made available to expedite the availability of information on the research discussed herein.

1

LA-UR -84-1319

CONF

Los Alamos National Laboratory is operated by the University of California for the United States Department of Energy under contract W-7405-ENG-36

CONF-840873--9

TITLE HYDROGEN DIFFUSION FLAMES BURNING IN A MARK-III CONTAINMENT DESIGN

LA-UR--84-1319

DE84 011411

AUTHOR(S) J. R. Travis

SUBMITTED TO Joint ANS/ASME Conference on Design, Construction, and Operation of Nuclear Power Plants, August 5-8, 1984, Portland, Oregon

Los Alamos Los Alamos National Laboratory
Los Alamos, New Mexico 87545

FORM NO 836 R4
ST NO 2629 6/81

HYDROGEN DIFFUSION FLAMES BURNING IN A MARK III CONTAINMENT DESIGN*

J. R. Travis

Theoretical Division, Group T-3
University of California
Los Alamos National Laboratory
Los Alamos, New Mexico 87545

ABSTRACT

For the first time, a time-dependent, fully three-dimensional analysis of hydrogen diffusion flames combusting in nuclear reactor containments has been performed. The analysis involves coupling an Eulerian finite-difference fluid dynamic technique with the global chemical kinetics of hydrogen combustion. The overall induced flow patterns are shown to be very complex and greatly influence the maximum wet-well temperatures and pressures and wall heat fluxes.

*Work performed under the auspices of the United States Nuclear Regulatory Commission.

I. INTRODUCTION

In response to the United States Nuclear Regulatory Commission, we have analyzed diffusion flames burning above the pool in the wet-well of the MARK III containment design. In this accident sequence, a transient event from 100% power is followed by loss of all coolant-injection capability. The reactor vessel remains pressurized as the coolant water in the reactor vessel begins to boil away. When the core becomes uncovered and heats up, after roughly 40 minutes into the accident, zirconium and steel oxidation leads to the generation of hydrogen which is then released through safety relief valves (SRV's) into the suppression pool. Under certain conditions, this release of hydrogen (e.g., with an ignition source) leads to the formation of diff sion flames above the release areas in the suppression pool. These flames may persist in localized regions above the suppression pool for tens of minutes and therefore could lead to overheating of nearby penetrations in the dry-well or wet-well walls. It is of most interest to calculate the temperature and pressure of the containment atmosphere in the wet-well region and the heat flux loads on the dry-well and wet-well walls up to 10m above the suppression pool surface. The major contribution; however, of this analysis is the calculation of the overall induced flow patterns which allows identification of oxygen starved regions and regions where diffusion flames may lift off the pool surface.

II. MATHEMATICAL MODEL

The partial-differential equations that govern the fluid dynamics and species transport and model the hydrogen combustion process are presented in this section.

A. The Mixture Equations

The mixture mass conservation equation is

$$\frac{\partial \rho}{\partial t} + \nabla \cdot (\rho \bar{u}) = 0 \quad ,$$

where

$\rho = \sum_{\alpha=1}^{4} \rho_\alpha$; ρ_α = macroscopic density of the individual species (H_2O, N_2, H_2 or O_2).

$\bar{u}$ = mass-average velocity vector.

The mixture momentum conservation equations are given by

$$\frac{\partial (\rho \bar{u})}{\partial t} + \nabla \cdot (\rho \bar{\bar{u}}\bar{\bar{u}}) = - \nabla p + \nabla \cdot \bar{\bar{\sigma}} + \hat{\rho} \bar{g} - \bar{D} \quad ,$$

where

p = pressure,

$\bar{\bar{\sigma}}$ = viscous stress tensor,

$\hat{\rho}$ = local density relative to the average density

$\bar{g}$ = gravitational vector, and

$\bar{D}$ = structural drag vector.

The coefficients of viscosity, μ and λ, which appear in the viscous stress tensor, e.g.,

$$\sigma_{rr} = 2\mu \frac{\partial u}{\partial r} - \lambda \nabla \cdot \bar{u} \quad ,$$

where λ is defined

$$\lambda = \frac{2}{3}\mu \quad ,$$

and μ is interpreted as the "eddy viscosity", are defined by the simple algebraic turbulence model

$$\nu = \mu/\rho = 1/40\ s\ \sqrt{2q} \quad .$$

In this model, s is equal to a length scale (1.50 m for these calculations) and $\sqrt{2q}$ is the turbulent energy intensity ($0.15|\bar{u}|$ for these calculations),

so

$$\mu = 0.56\ \rho|\bar{u}| \quad .$$

The structural drag vector is given by

$$\bar{D} = C_D \rho(\text{Area/Volume})\bar{u}|\bar{u}| \quad ,$$

where

$$\text{Area/Volume} = \frac{\text{structure area}}{\text{structure volume}} \quad ,$$

and

$$C_D = 1.$$

The mixture internal energy density equation is

$$\frac{\partial(\rho I)}{\partial t} + \nabla\cdot(\rho I\bar{u}) = -\ p\nabla\cdot\bar{u} + \nabla\cdot(\kappa\nabla T) + Q \quad ,$$

where

I = mixture specific internal energy

κ = "eddy conductivity",

T = mixture temperature, and

Q = energy source and/or sink per unit volume and time.

The specific internal energy is related to the temperature by

$$I = \sum_{\alpha=1}^{4} X_\alpha (I_o)_\alpha + \sum_{\alpha=1}^{4} X_\alpha \int_{T_o}^{T} (C_v)_\alpha \, dT \quad ,$$

where X_α is the mass fraction, $(I_o)_\alpha$ is the specific internal energy at the reference temperature, T_o, for specie α and the specific heats at constant volume, $(C_v)_\alpha$, have been represented over the temperature range (200, 2500) degrees Kelvin by the linear approximation

$$(C_v)_\alpha = A_\alpha + B_\alpha T \quad .$$

The equation-of-state for the average fluid pressure P_o is given by the ideal gas mixture equation

$$P_o = T \sum_{\alpha=1}^{4} R_\alpha \rho_\alpha \quad ,$$

where R_α is the gas constant for specie α. The eddy conductivity is found by assuming the Prandtl Number, Pr, equal to unity, i.e.,

$$Pr = \frac{C_p \mu}{\kappa} = 1 \quad ,$$

thus

$$\kappa = C_p \mu \quad ,$$

where

$$C_p = \sum_{\alpha=1}^{4} X_\alpha (C_p)_\alpha = \sum_{\alpha=1}^{4} X_\alpha R_\alpha + (C_v)_\alpha \quad .$$

The energy source/sink term has several contributions: (1) chemical energy of hydrogen combustion, Q_f; (2) heat transfer to the structure, Q_s; and if the computational zone is adjacent to a containment wall there is heat transfer to the wall, Q_w; therefore,

$$Q = Q_f - Q_s - Q_w \quad ,$$

where

$Q_f = .85 Q_c$ = 85% of the chemical energy per unit volume and time, Q_c, produced by hydrogen combusting (the other 15% of the chemical energy is radiated to the wet-well and dry-well walls),

$Q_s = h_s(\text{Area/Volume})(T - T_s)$, and

$Q_w = h_w(A_w/V)(T - T_w)$.

In the above relations, h_s is the structural heat transfer coefficient, 1000 $W/m^2 \cdot K$ for these analyses, h_w is the wall heat transfer coefficient, 20 $W/m^2 \cdot K$ for these calculations, T_s is the structure temperature, T_w is the wall temperature, A_w is the wall surface area, and V is the computational zone volume adjacent to the wall. Wall heat transfer is calculated by

$$kA_w \frac{\partial T_w}{\partial r} + h_w A_w (T - T_w) + Q_r = 0 \quad ,$$

where

Q_r = total amount of energy per unit time radiated from all hydrogen flames to a particular computational zone wall area, and

k = wall thermal conductivity 0.81 W/m·K for these calculations .

We have assumed a simple penetration model for calculating the wall heat flux. Using the analytic solution for a transient thermal wave penetrating into a semi-infinite medium, we can write

$$\frac{\partial T_w}{\partial r} = \frac{T_w - T_{ref}}{\sqrt{\pi \beta t}} \quad ,$$

where T_{ref} is the deep wall reference temperature, and

β = thermal diffusivity, $4.9 \times 10^{-7} \frac{m^2}{s}$ for these analyses .

B. The Species Transport Equations

The dynamics of the individual species are determined by

$$\frac{\partial \rho_{H_2O}}{\partial t} + \nabla \cdot (\rho_{H_2O} \bar{u}) - \nabla \cdot \rho \gamma V \frac{\rho_{H_2O}}{\rho} = S_{H_2} + S_{O_2} \quad ,$$

$$\frac{\partial \rho_{N_2}}{\partial t} + \nabla \cdot (\rho_{N_2} \bar{u}) - \nabla \cdot \rho \gamma V \frac{\rho_{N_2}}{\rho} = 0 \quad ,$$

$$\frac{\partial \rho_{H_2}}{\partial t} + \nabla \cdot (\rho_{H_2} \bar{u}) - \nabla \cdot \rho \gamma V \frac{\rho_{H_2}}{\rho} = - S_{H_2} \quad ,$$

and

$$\frac{\partial \rho_{O_2}}{\partial t} + \nabla\cdot(\rho_{O_2}\bar{u}) - \nabla\cdot\ \rho\gamma\nabla\frac{\rho_{O_2}}{\rho} = -S_{O_2} \quad ,$$

where the "eddy diffusivity", γ, is determined by setting the Schmidt Number to unity, $\gamma = \mu/\rho$, and S_{H_2} and S_{O_2} are determined by the chemical kinetics presented below. Summing the above species transport equations results in the mixture mass conservation equation.

C. Chemical Kinetics

We are employing global chemical kinetics in which the only reaction modelled is

$$2H_2 + O_2 \overset{\dot{\omega}}{\rightarrow} 2H_2O + Q_c \quad .$$

Hydrogen combustion proceeds by means of many more elementary reaction steps and intermediate chemical species. The chemical reaction time scale is, however, very short compared with fluid dynamic motions and meaningful calculations can be accomplished using this simplified global chemical kinetics scheme.[2]
Here, Q_c is the chemical energy of combustion per unit volume and time, i.e.,

$$Q_c \frac{W}{cm^3} = 4.778 \times 10^5 \frac{J}{mole}\ \dot{\omega}\ \frac{mole}{m^3\cdot s} \quad .$$

The reaction rate, $\dot{\omega}$, is modelled by Arrenhius kinetics as

$$\dot{\omega} = C_f \frac{\rho}{M}_{H_2} \frac{\rho}{M}_{O_2} \exp(-10^4/T) \quad ,$$

where M is the molecular weight and $C_f = 3.3 \times 10^5 \ \frac{m^3}{mole - s}$. Now, the source terms S_H and S_{O_2} are found by

$$S_{H_2} = 2M_{H_2}\dot{\omega} \ ,$$

and

$$S_{O_2} = M_{O_2}\dot{\omega} \ .$$

III. SOLUTION PROCEDURE

The above equations are written in finite-difference form for their numerical solution. The nonlinear finite-difference equations are then solved iteratively using a point relaxation method. Since we are interested in low-speed flows where the propagation of pressure waves need not be resolved, we are therefore utilizing a modified ICE[1] solution technique where the species densities are functions of the containment pressure, and not of the local pressure. Time-dependent solutions can be obtained in one, two, and three space dimensions in plane and in cylindrical geometries, and in one- and two-space dimensions in spherical geometries. The geometric region of interest is divided into many finite-sized space-fixed zones called computational cells that collectively form the computing mesh. Figure 1 shows a typical computational cell with the velocities centered on cell boundaries. All scalar quantities, such as I, p, and ρ_α's, are positioned at the cell-center designated (i,j,k). The finite-difference equations for the quantities at time $t=(n+1)\delta t$ form a system of coupled, nonlinear algebraic equations.

The solution method starts with the explicit calculation of the chemical kinetics yielding the source terms in the species transport equations and

specific internal energy density equation. Next, the convection, viscous stress tensor, gravity, and drag terms are evaluated in the mixture momentum equations and an estimate of the time advanced velocities is obtained. The solution method then proceeds with the iteration phase:

(1) The $(\rho'_\alpha)^{n+1}$'s are found from the species transport equations using the latest iterates for $(\rho)_\alpha^{n+1}$ and $\bar{u}^{n+1}$.

(2) The global or average fluid pressure, P_o^{n+1} is determined by integrating the equation-of-state over the computational mesh.

(3) The equation-or-state is modified slightly to find the mixture density using the $(\rho'_\alpha)^{n+1}$'s and P_o^{n+1} from steps (1) and (2)

$$\rho_{i,j,k}^{n+1} = \frac{P_o^{n+1} \sum_{\alpha=1}^{3} (\rho'_\alpha)_{i,j,k}^{n+1}}{T_{i,j,k}^{n} \sum_{\alpha=1}^{3} R_\alpha \, (\rho'_\alpha)_{i,j,k}^{n+1}} \quad .$$

(4) With $\rho_{i,j,k}^{n+1}$ [from step (3)] and the latest iterates for $\bar{u}^{n+1}$ the residual, $D_{i,j,k}$, in the mixture mass equation is calculated. If the convergence criterion is met, for example $|D_{i,j,k}| < \varepsilon$ where $\varepsilon = 10^{-4} \times \rho_{i,j,k}^{n}$, then no adjustment is made to the local pressure, $p_{i,j,k}^{n+1}$, and the velocities $\bar{u}_{i,j,k}^{n+1}$ for cell (i,j,k). When the convergence criterion is met for all cells in the computational mesh, the iteration phase of the cycle is complete.

(5) For any cell that the criterion is not met, the local pressure is changed by an amount

$$\delta p_{i,j,k} = - \frac{\Omega \, D_{i,j,k}}{\frac{\partial D}{\partial p}_{i,j,k}} \quad ,$$

where

$$\frac{\partial D}{\partial p}_{i,j,k} = \frac{2\delta t^2}{\delta r^2 + (r_i \delta\theta)^2 + \delta z^2} \quad ,$$

and Ω is a constant over-relaxation factor selected $1.0 \leq \Omega < 2.0$, and the momenta are changed due to the new pressure gradient. The velocities are found by simply dividing the momenta by the updated densities. Steps (1) - (5) are repeated until the convergence criterion as presented in step (4) is satisfied on the entire computational mesh. After the iteration phase is complete, the specific internal energy density equation is evaluated and the computational time step is finished with the advancement of the time step.

IV. GEOMETRY, COMPUTATIONAL MESH, AND INITIAL AND BOUNDARY CONDITIONS

The MARK III containment design is shown schematically in Fig. 2. We are only concerned with the containment volume above the water level so we approximate the containment with the configuration presented in Fig. 3, which has the same atmospheric containment volume as that of Fig. 2. The outer vertical containment wall (wet-well wall) is concrete 0.75 m (2.5 feet) thick and the inner vertical wall (dry-well wall) is concrete 1.5 m (5 feet) thick. The annular region between these two walls is called the wet-well. Hydrogen spargers or sources are actually at the bottom of the suppression pool within 3 m of the inner wall. The nine sources can be thought of as circular, 3 m diameter, centered azimuthally at 16, 48, 88, 136, 152, 184, 256, 288, and 328 degrees. Fig. 4 gives the idea of the sources relative to the wet-well and the containment walls.

The geometry as shown in the two perspective views of Figs. 5 and 6 indicates that true three-dimensionality of the containment. The hydrogen sources are shown at the bottom as dark rectangular regions. The cylindrical computa-

tional mesh approximating this geometry is presented in Fig. 7 which shows each of the computing zones. A pie shaped region of the computing mesh indicating the dimensions is presented in Fig. 8. Hydrogen enters the computing mesh at the bottom (J=2) of specific cells in the annular ring (I=8) with a temperature equalling 71°C and pressure equalling 10^5 Pa. The initial conditions in the containment is dry air at 21°C and 10^5 Pa. The azmuthal positions of the hydrogen sources within the ring I=8 are specified at K = 4, 6, 8, 13, 15, 16, 20, 22, and 24 which corresponds to computational zones centered at 322.5, 292.5, 262.5, 187.5, 157.5, 142.5 82.5, 52.5, and 22.5, respectively. The mass flow rate of 100 lb/min is distributed equally among the nine sources.

There are tremendous heat sinks in the containment e.g., 2.2×10^6 kg steel with heat transfer surface area equalling 2.7×10^4 m^2, from which an average surface area per unit volume can be found. The structural heat transfer and drag formulations both use this average value to compute heat and momentum exchange, respectively, within a computational zone.

TABLE I

AZMUTHAL POSITIONS OF THE HYDROGEN SOURCES WITHIN RING I=8

Case "B"		Case "C"		Case "3"	
Azmuthal Positions		Azmuthal Positions		Azmuthal Position	
K	Degrees	K	Degrees	K	Degrees
4	322.5	4	322.5	22	52.5
6	292.5	6	292.5		
8	262.5	8	262.5		
13	187.5	13	187.5		
16	142.5	15	157.5		
20	82.5	16	142.5		
21	67.5	20	82.5		
22	52.5	22	52.5		
24	22.5	24	22.5		

V. RESULTS

Fig. 9 displays velocity vectors in an unwrapped (constant radius vs. height) configuration. The radius is at the radial center of the hydrogen source cells (I=8), which can be seen at the bottom of each plot by the openings. For example, there is a double source between 135 and 165 degrees and seven single sources distributed along the azmethal dimension. With nine distributed sources, and distributed as they are, Fig. 9 shows the development of very strong buoyancy driven flows in the partial hot chimney at 45 degrees and the full hot chimneys at 135 and 315 degrees. A cold chimney (downflow) develops at 225 degrees completing the convective loops. The partial hot chimney (45 degrees) is blocked by a concrete floor about half way to the top and is diverted toward the outer wall and upward around the enclosed volumes shown in this figure. The horizontal lines designate concrete floors where no mass, momentum or energy is allowed to flux across these lines. Thus we see the hot products of combustion beneath the floors at say 270 degrees convecting horizontally and contributing to the full hot chimney at 315 degrees. Maximum gas temperatures are generally found in regions of multiple sources and beneath concrete floors as depicted in Fig. 10.

Early in the calculation, 120s, most of the hydrogen combusts in the inlet computational zone as shown by the hydrogen density contour plot of Fig. 11. This is confirmed by the chemical energy contour plot (Fig. 12) which shows the energy of combustion in the nine source inlet regions and the oxygen density contour plot (Fig. 13) showing low values near combustion regions and high values in the cold chimney (225 degrees). At later times (1410s), Figs. 14, 15, 16, and 17 show the same overall flow pattern, but only hydrogen sources near the cold chimney are continuing to combust in the inlet regions. The others which have become oxygen starved are combusting higher up in the wet-well. This is better shown perhaps in Fig. 18 where high gas temperatures are found far above the pool surface.

Summary results are presented in the next figures. Figure 19 shows the maximum and minimum wet-well temperatures and containment atmosphere pressure.

Note that the maximum temperature would always be the adiabatic flame temperature for the composition of gases at that particular time. We correctly calculate the adiabatic flame temperature; however, because of the coarseness of the computational mesh, the temperature of any zone in which combustion is taking place will always be lower than the actual adiabatic flame temperature. Mass histories for H_2O, H_2, and O_2 are also included. Note that at roughly 1600s, oxygen is totally depleted in the containment. Spatial distributions for heat fluxes to the inner and outer wet-well walls at 10 feet and 30 feet above the pool surface are presented in Fig. 20 for various times (60, 150, 600, and 1800 seconds). The hydrogen sparger or source azmuthal positions are indicated on each figure. Maximum heat flux values correspond one for one at the sparger locations. For azmuthal locations 142.5 and 292.5 degrees where large values of the heat flux occur, we have given heat flux histories at the 10 feet and 30 feet above the suppression pool surface for both inner and outer walls. The heat fluxes on the inner wall peak early and then decrease as heat is convected to other regions of the containment. Most of the heat transferred to the outer wall is radiated to these surfaces from the burning hydrogen.

Without a flame model or resolving flame details with a finely zoned computational mesh, it is impossible for us to supply details about the flame such as flame height, flame width and flame angle. We can say; however, that most of the combustion takes place in the inlet cell (flame height 6m), as long as there is sufficient oxygen for combustion. Once flames become oxygen starved, then it is possible for flames to lift off the water surface and burn higher in the wet-well, perhaps even reattaching to the water surface as more oxygen is supplied by convection.

VI. CONCLUSIONS

This is the most sophisticated analysis to this date of diffusion flames in reactor containments. Improvements can be made in the wall heat transfer treatment, the amount of radiant heat transferred from each chemical energy source, the turbulence model and the chemical kinetics representation; however, the effects of these phenomena are accounted for, and the fluid dynamics of the overall induced flow patterns are relatively insensitive to changes in these parameters. In strictly conserving mass, momentum, and energy throughout the computational mesh, these time-dependent, fully three-dimensional calculations should be considered benchmarks analyses.

VII. ACKNOWLEDGMENTS

It is a pleasure to express appreciation to T. D. Butler, J. K. Dukowicz, F. H. Harlow, and P. J. O'Rourke for their helpful discussions throughout this work.

VIII. REFERENCE

1. F. H. Harlow and A. A. Amsden, "Numerical Fluid Dynamics Calculation Method for All Flow Speeds," J. Comput. Phys. 8, 197 (1971).

2. T. D. Butler, L. D. Cloutman, J. K. Dukowicz, and J. D. Ramshaw, "Multidimensional Numerical Simulation of Reactive Flow in Internal Combustion Engines," Prog. Energy Combust. Sci. 7, 293 (1981).

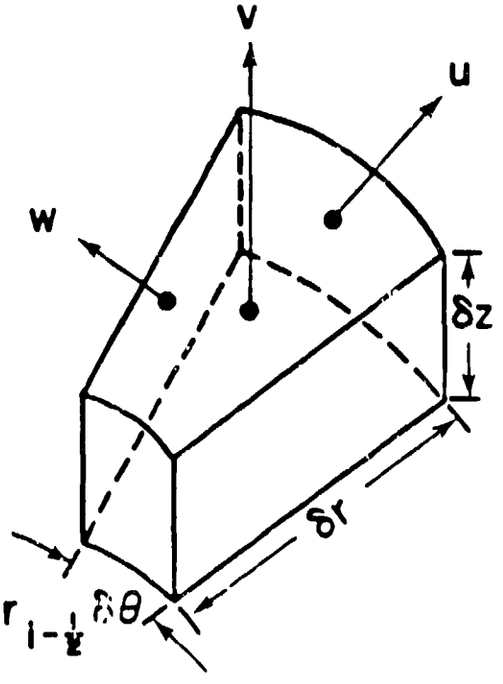

Fig. 1.
Locations of velocity components for a typical cell in cylindrical geometry.

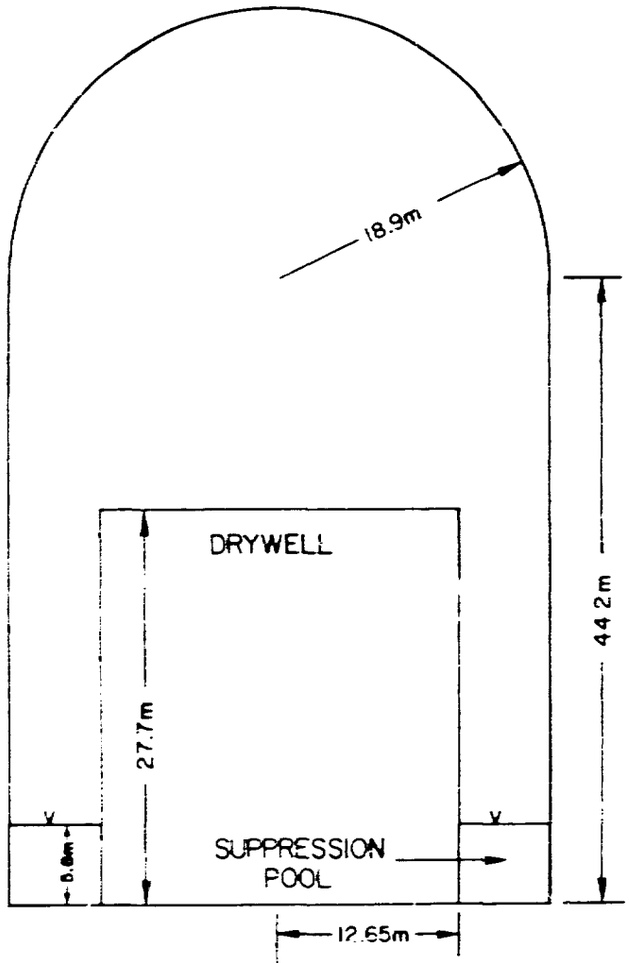

Fig. 2. Schematic View of the MARK-III Containment Design showing the Suppression Pool and the Wet-well (Annular Region above the Pool)

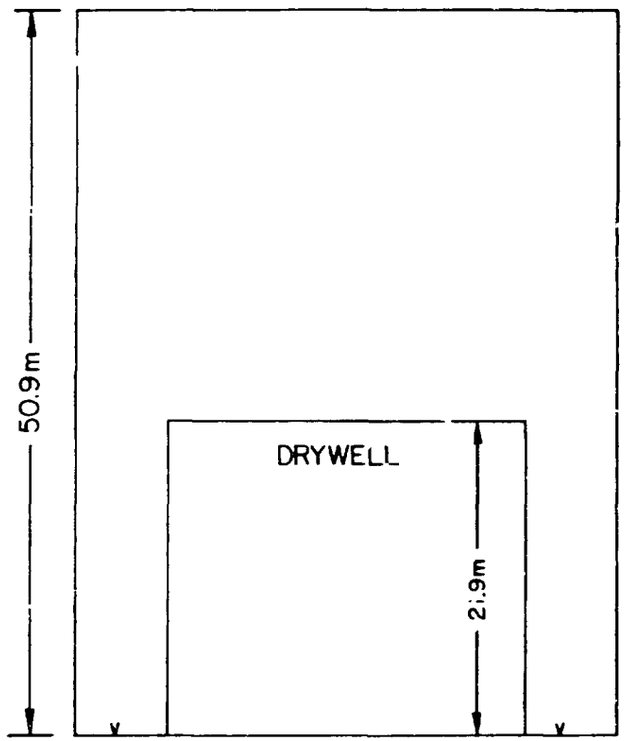

Fig. 3. Schematic View of the MARK-III Containment Design showing the geometry used in the Calculation. Note that the Containment Volumes are Equal are Equal in Figs. 2 and 3.

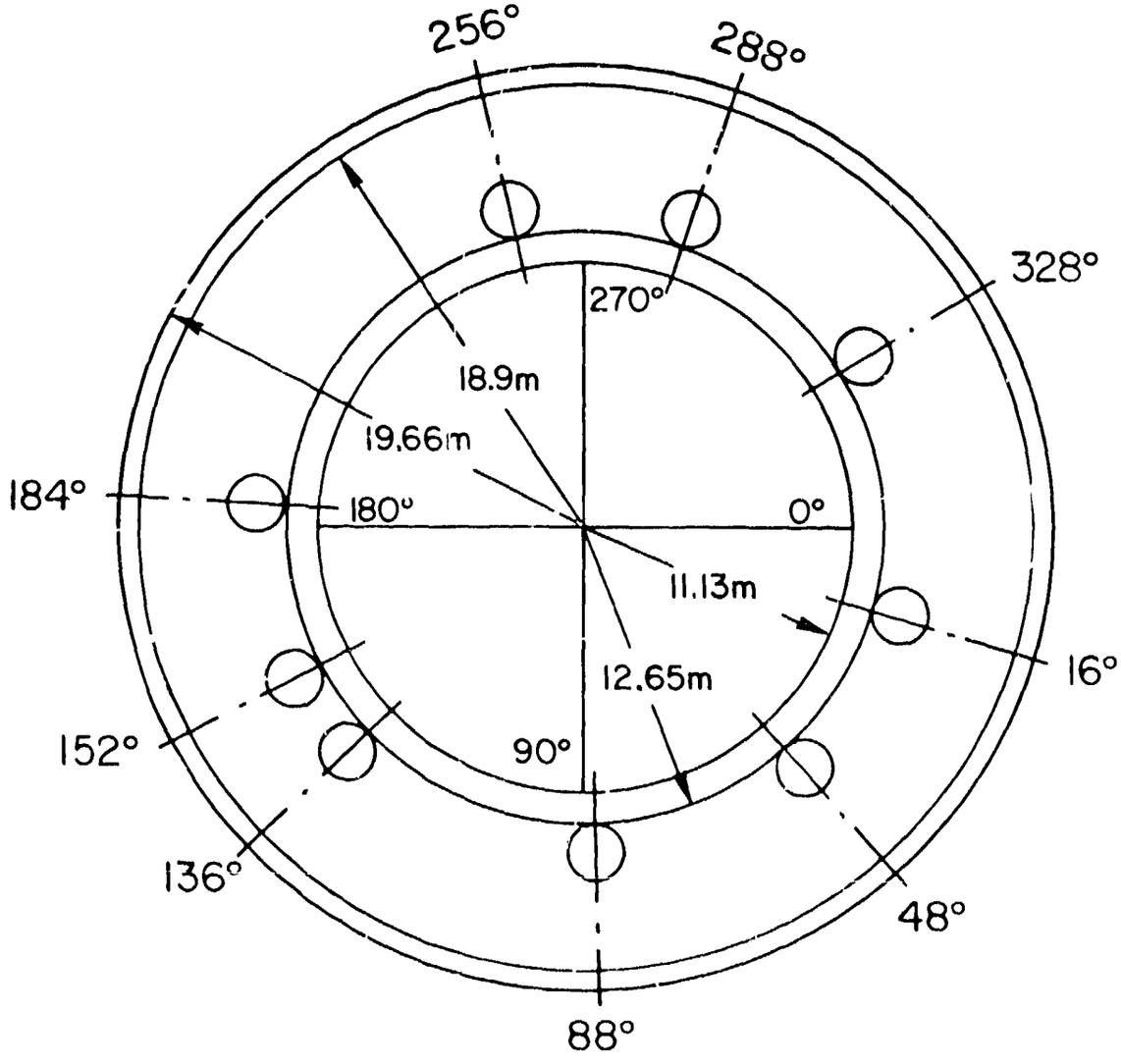

Fig. 4. Schematic View of the MARK-III Containment Design showing the Hydrogen Spargers (sources) Relative to the Wet-Well.

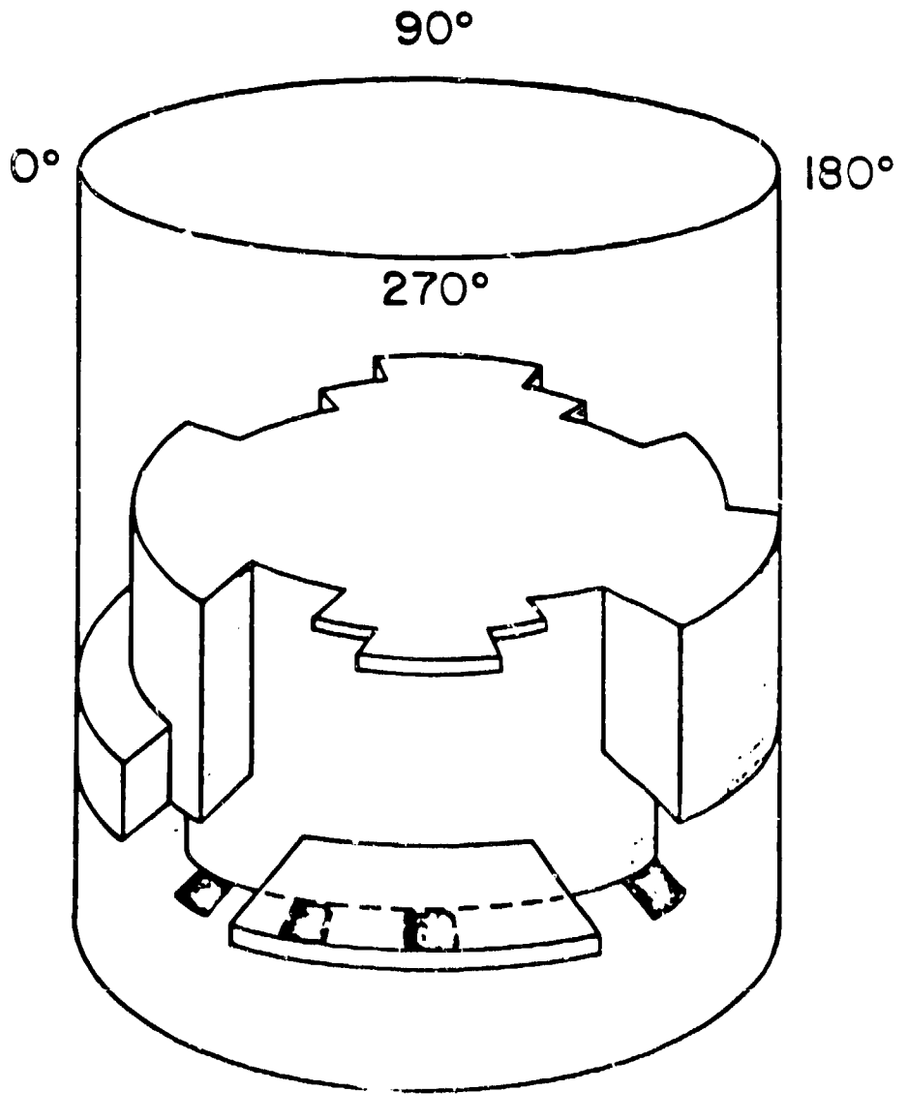

Fig. 5.
Perspective Front View of Containment showing Excluded Volumes, Concrete Floors, and Locations of Hydrogen Sources for Case C.

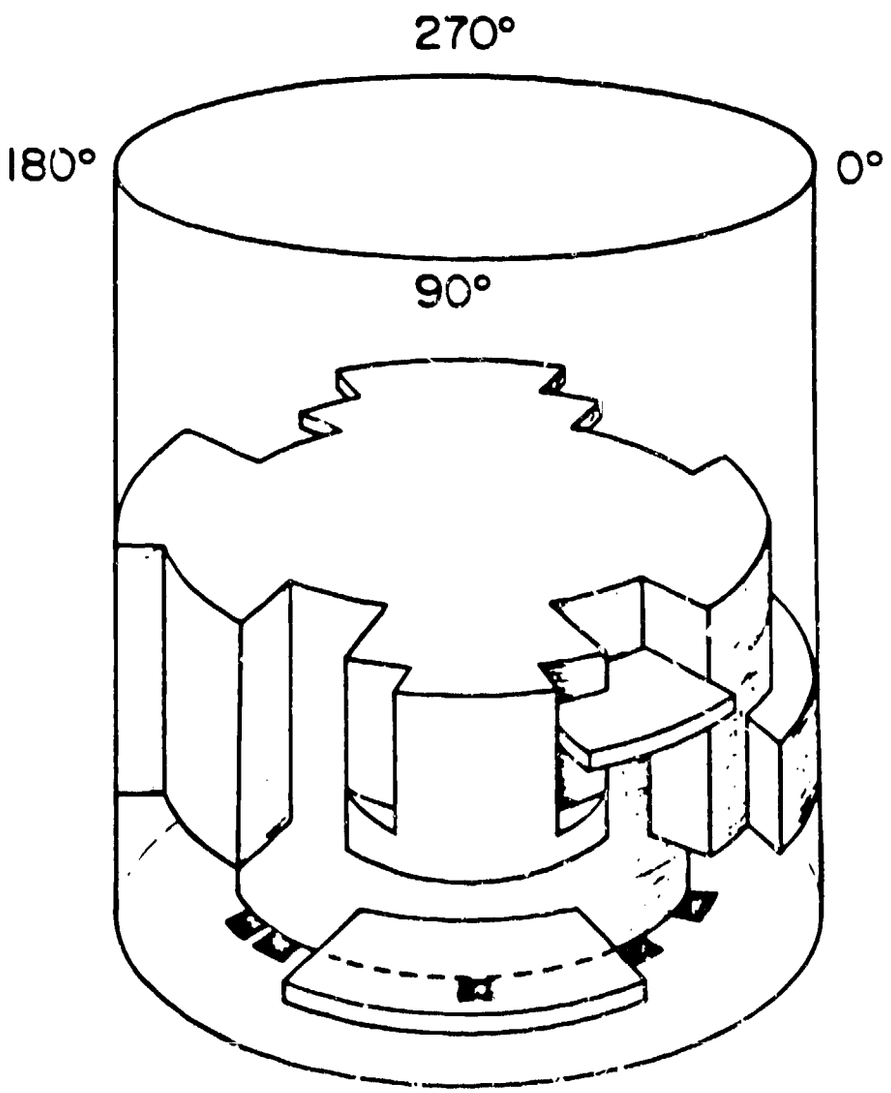

Fig. 6.
Perspective Back View of Containment Showing Excluded Volumes, Concrete Floors and Locations of Hydrogen Sources for Case C.

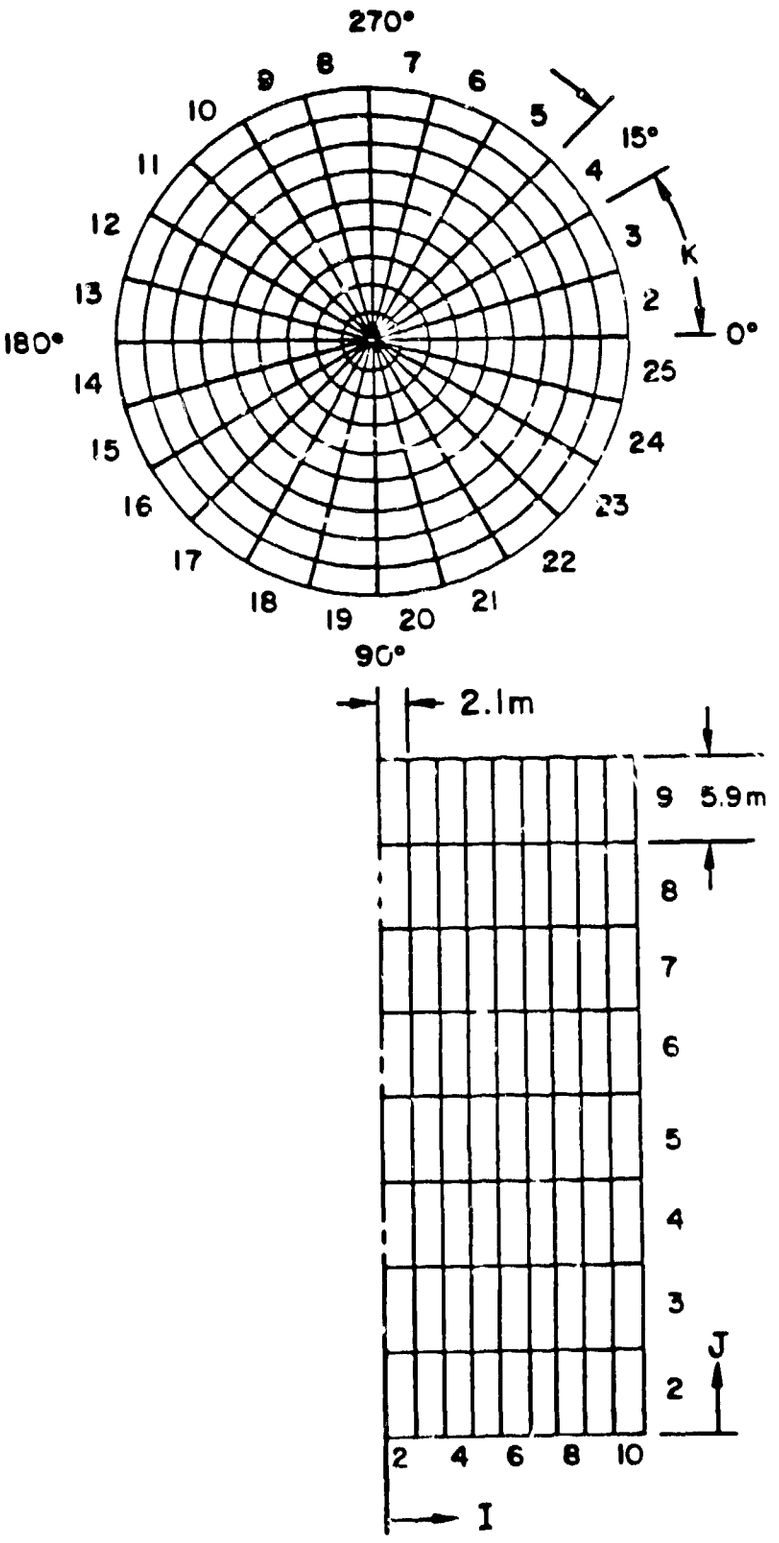

Fig. 7.
Computing Mesh for Containment Geometry.

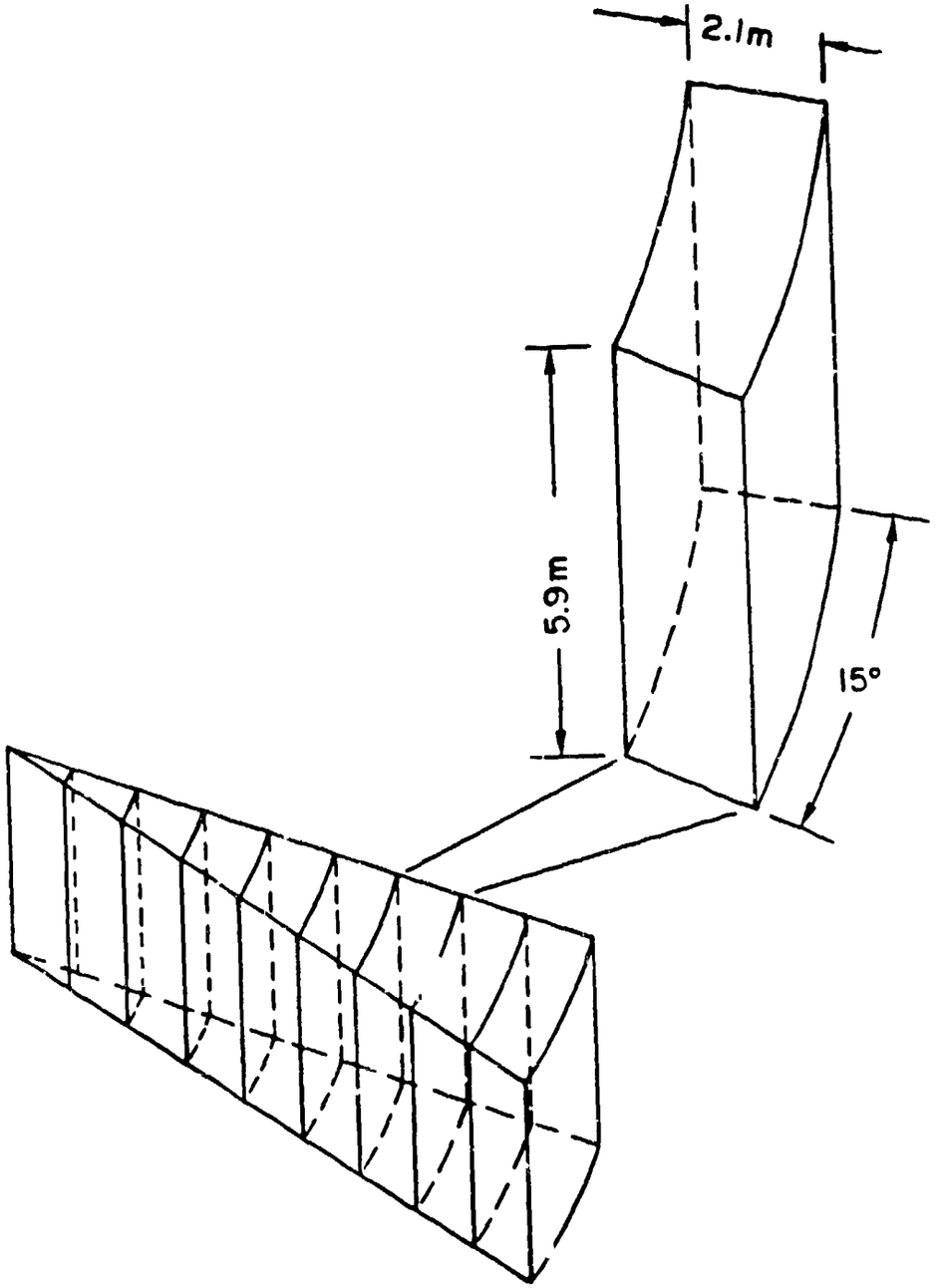

Fig. 8.
Perspective View of a Pie Shaped Zone within the Computing Mesh.

Fig. 9. Unwrapped (constant radius, I=8 vs. axial dimension, z) Velocity Vectors at 120s. V_{max}=7.4 m/s and W_{max}=2.9 m/s

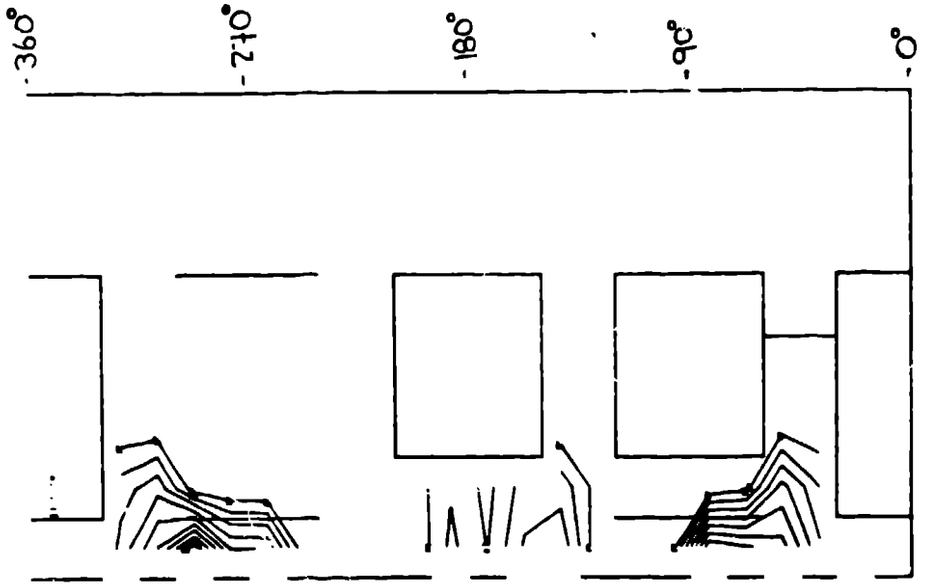

Fig. 10. Unwrapped (constant radius, I=8 vs. axial dimension, z) Gas Temperature Contours at 120s. T_{max}=1233K and T_{min}=399K

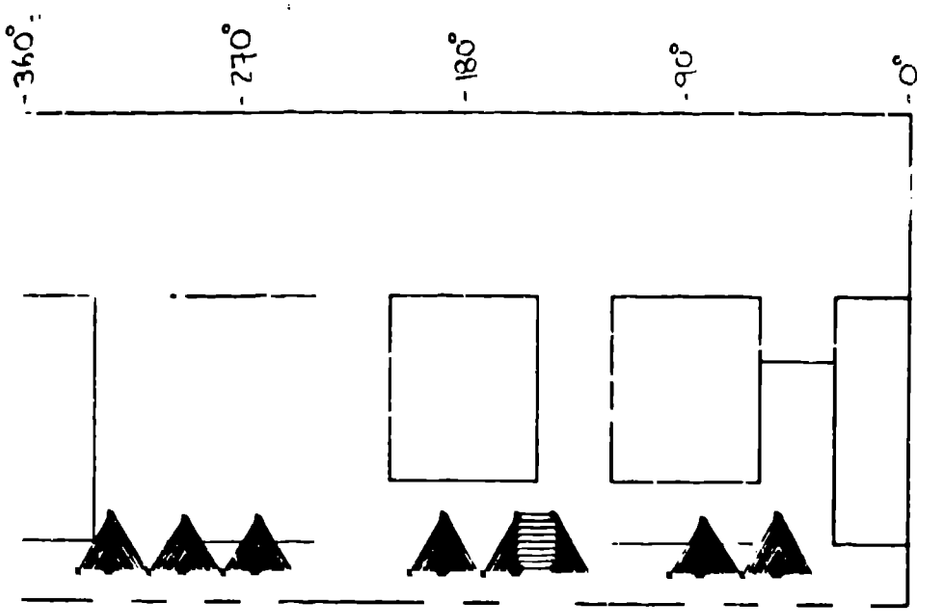

Fig. 11. Unwrapped (constant radius, I=8 vs. axial dimension, z) Hydrogen Density Contours at 120s.

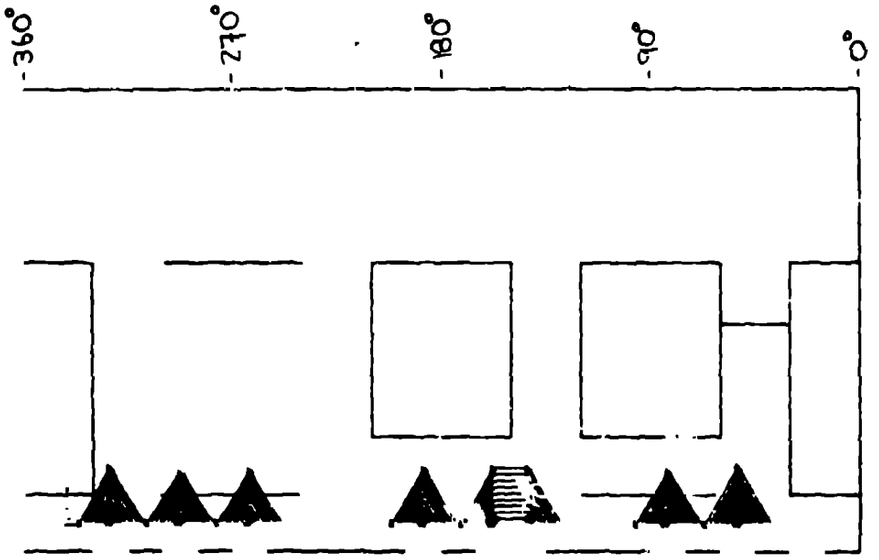

Fig. 12. Unwrapped (constant radius, I=8 vs. axial dimension, z) Chemical Energy of Combustion Contours at 120s.

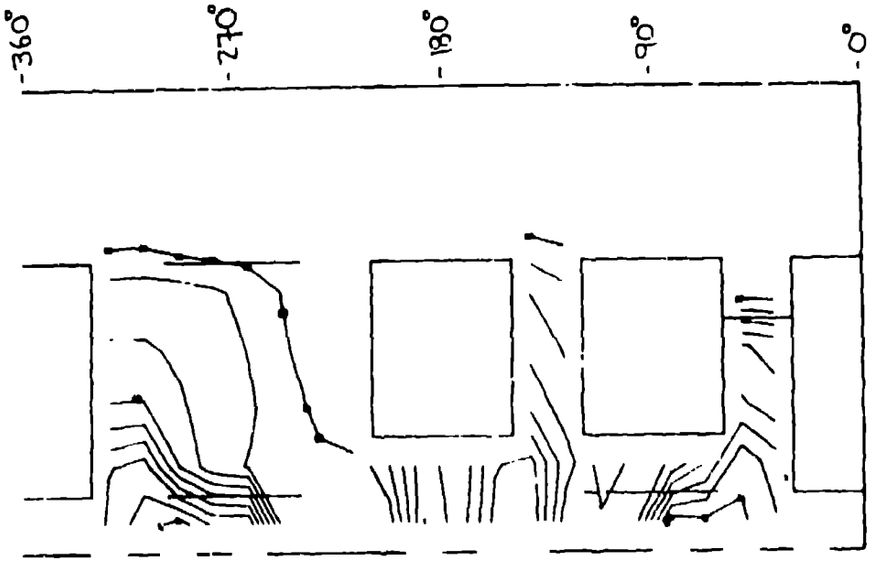

Fig. 13. Unwrapped (constant radius, I=8 vs. axial dimension, z) Oxygen Density Contours at 120s.

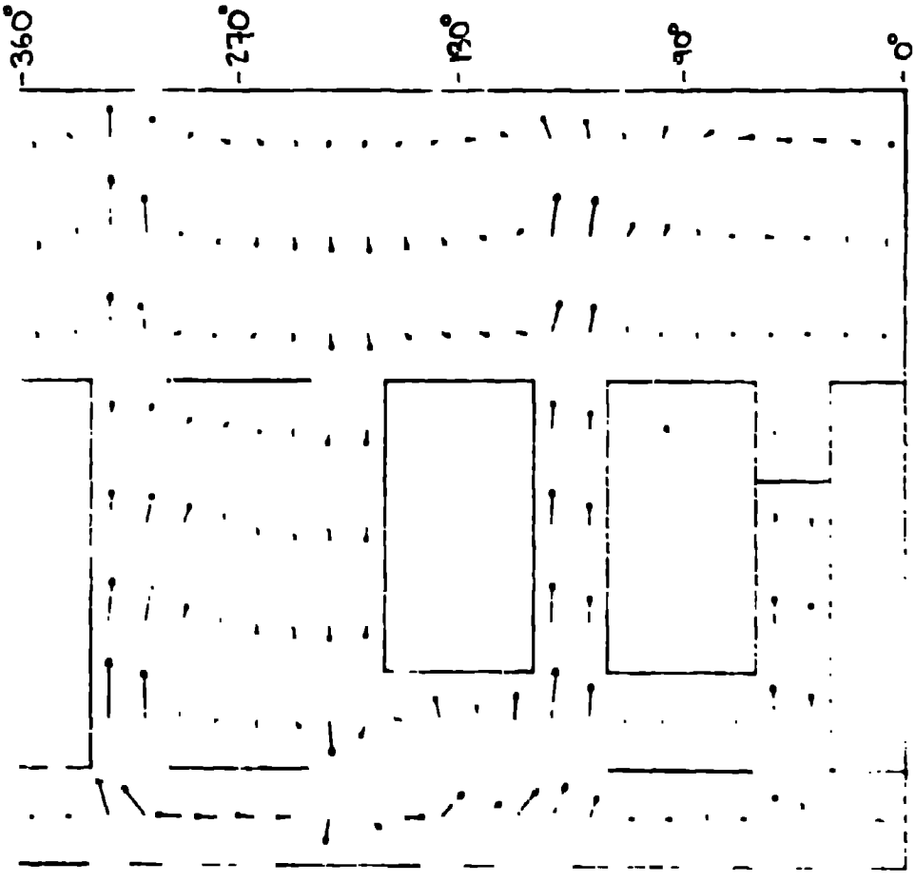

Fig. 14. Unwrapped (constant radius, r=8 vs. axial dimension, z) Velocity Vectors at 1410s. V_{max}=3.7 m/s and W_{max}=2.2 m/s

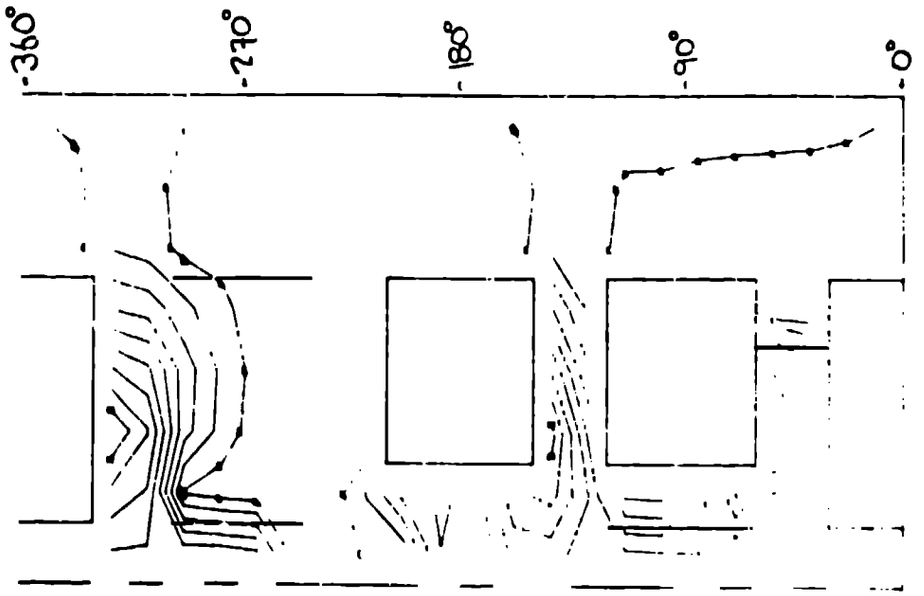

Fig. 15. Unwrapped (constant radius, I=8 vs. axial dimension, z) Gas Temperature Contours at 1410s. T_{max}=732K and T_{min}=346K

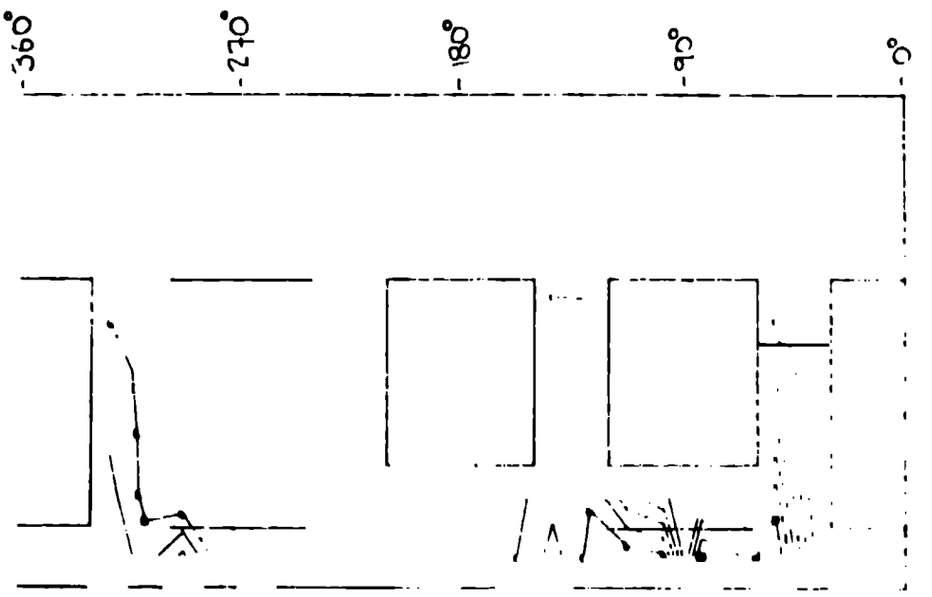

Fig. 16. Unwrapped (constant radius, I=8 vs. axial dimension, z) Hydrogen Density Contours at 1410s.

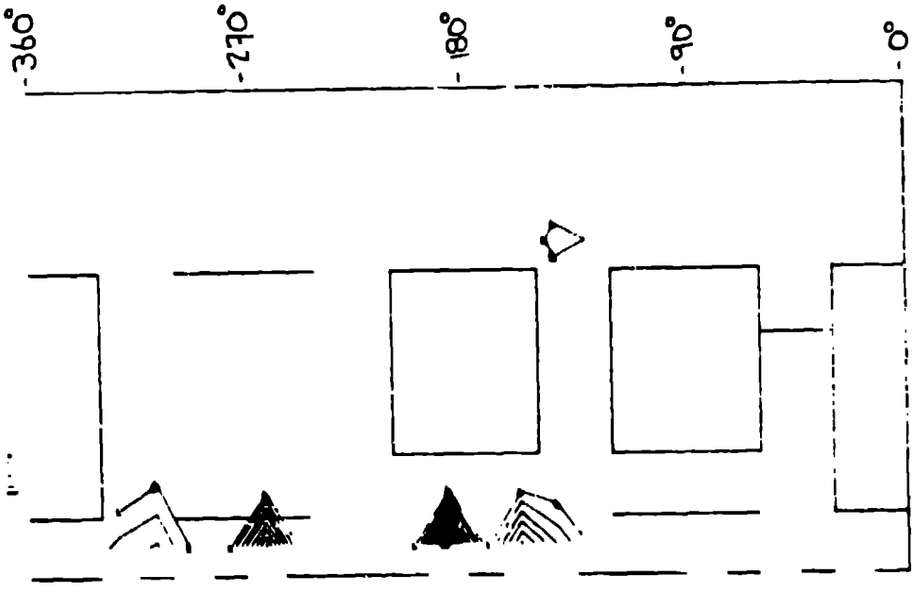

Fig. 17. Unwrapped (constant radius, I=8 vs. axial dimension, z) Chemical Energy of Combustion Contours at 1410s.

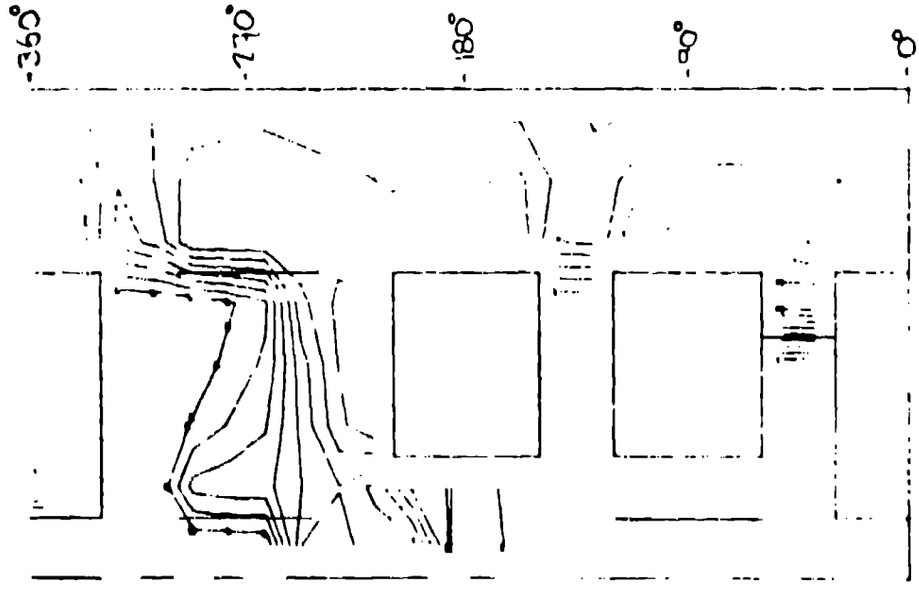

Fig. 18. Unwrapped (constant radius, I=8 vs. axial dimension, z) Oxygen Density Contours at 1410s.

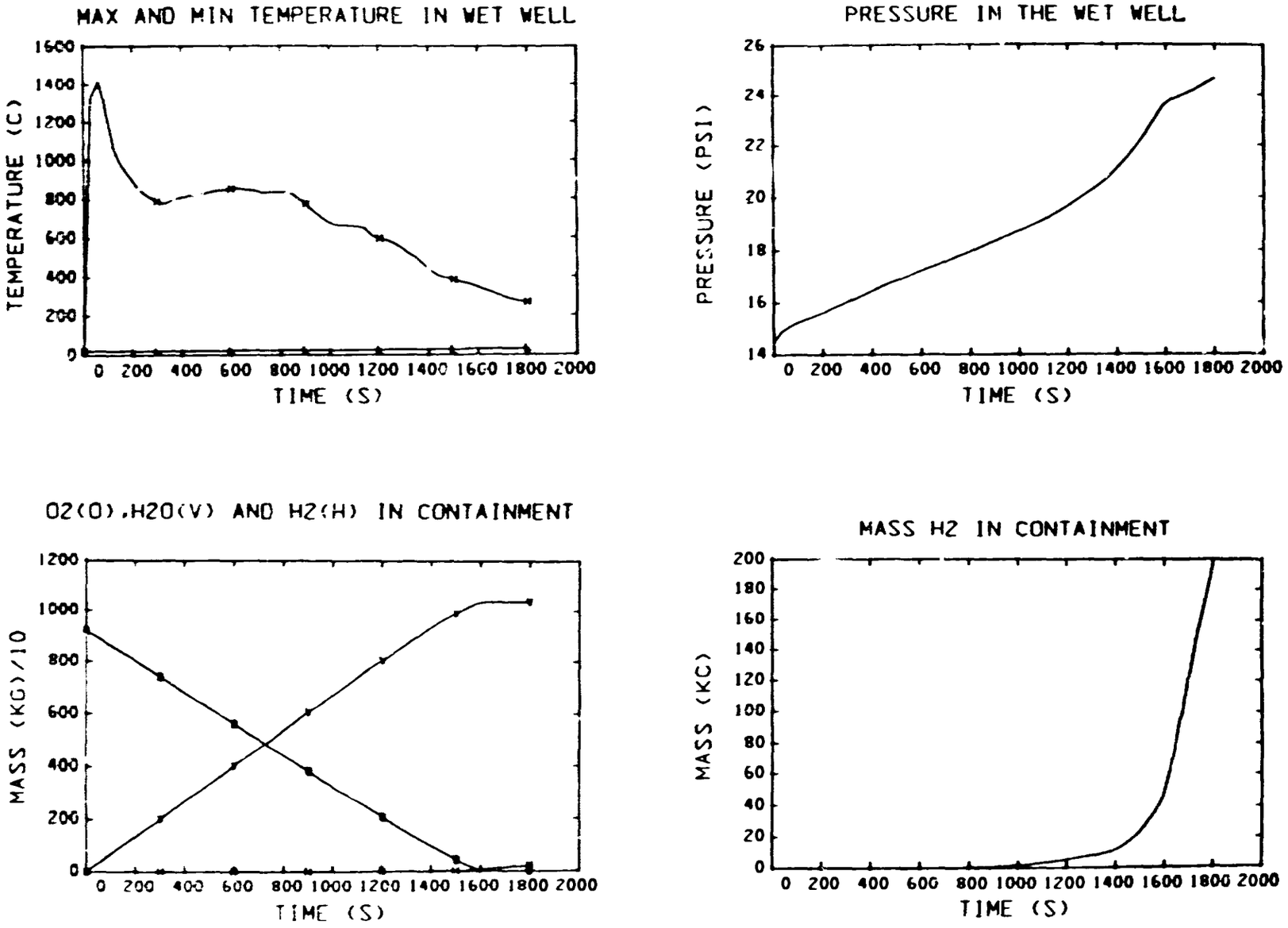

Fig. 19. Summary Results: Maximum and Minimum Atmospheric Wet-Well Temperatures (upper left), Maximum Containment Pressure (upper right), O_2, H_2O, and H_2 Mass in Containment (lower left), and H_2 Mass in Containment (lower right)

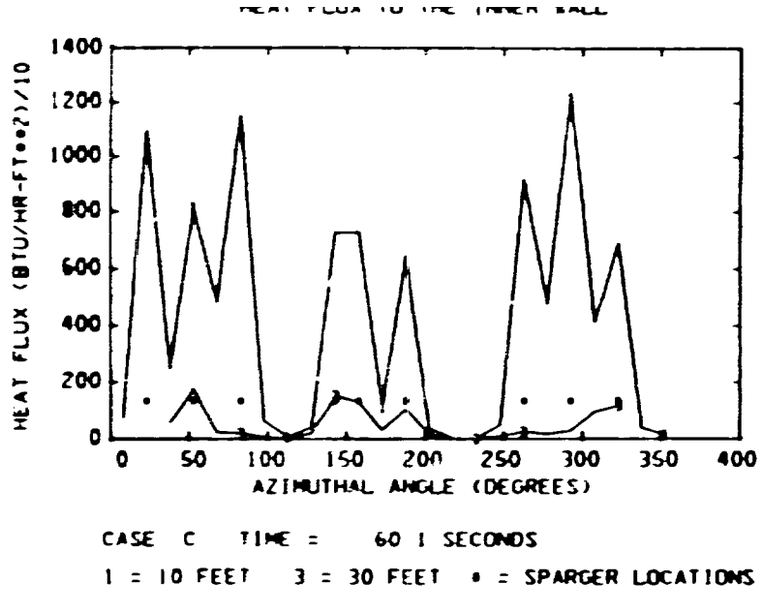

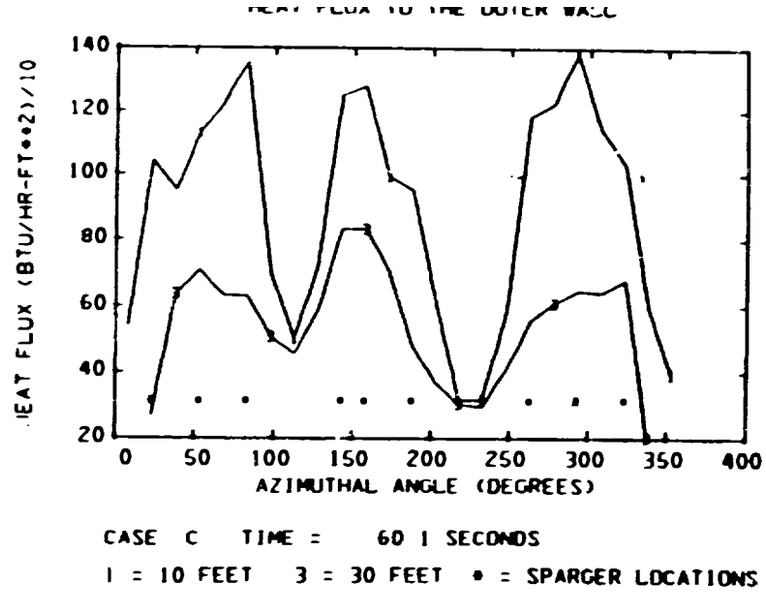

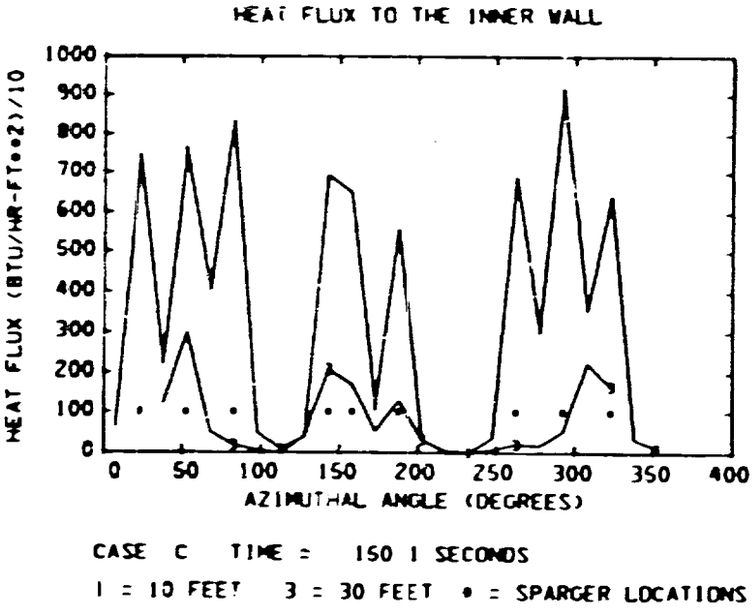

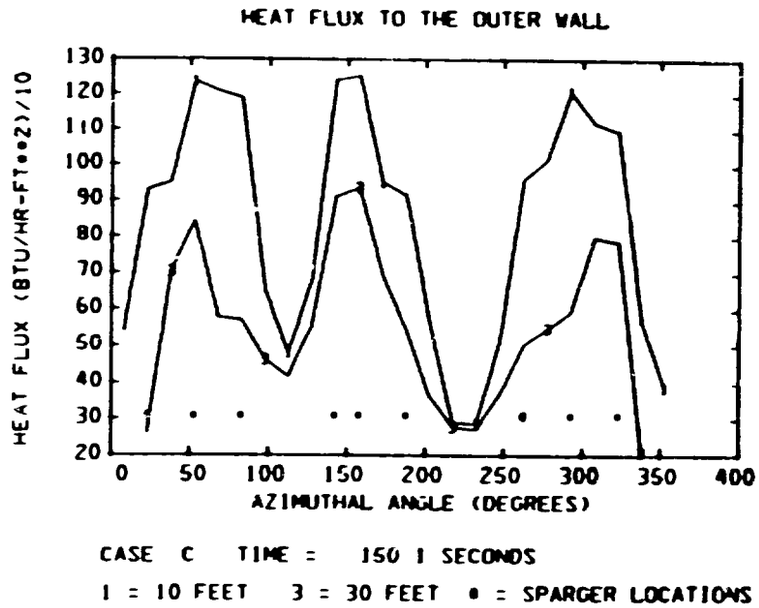

Fig. 20. Heat Flux to the Wet-Well Walls as a function of Azimuthal Position at Selected Times (60s top and 150s bottom).

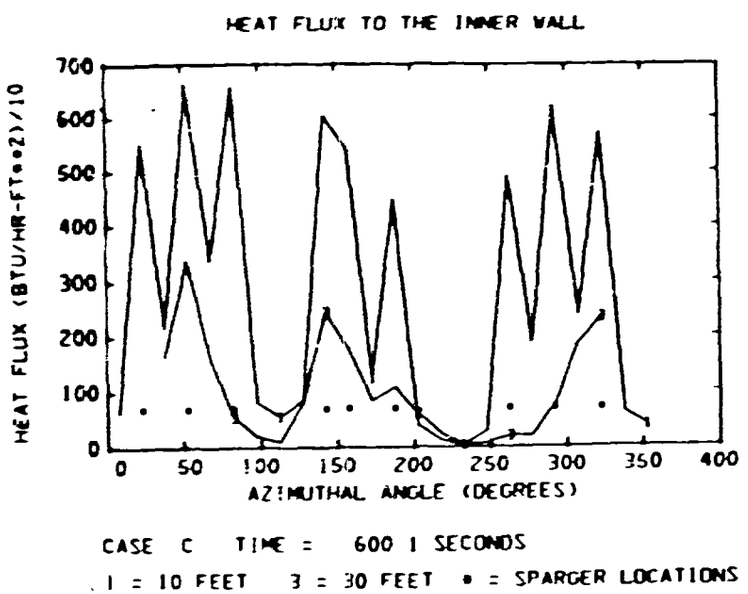

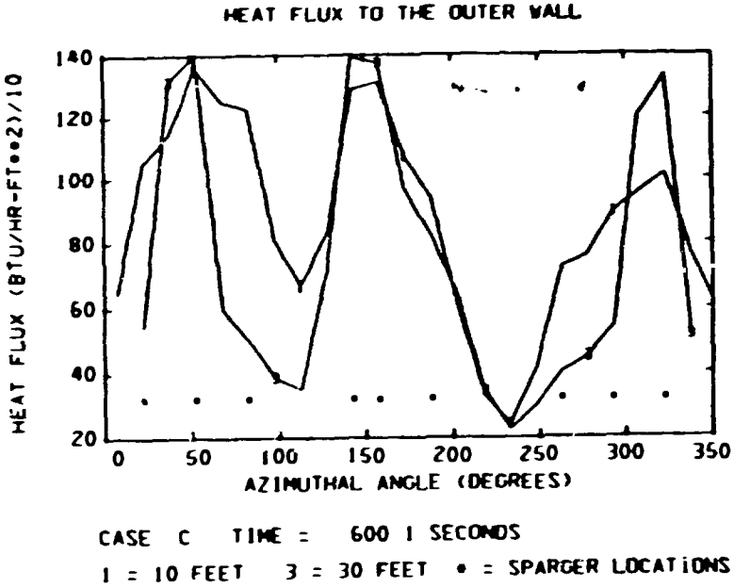

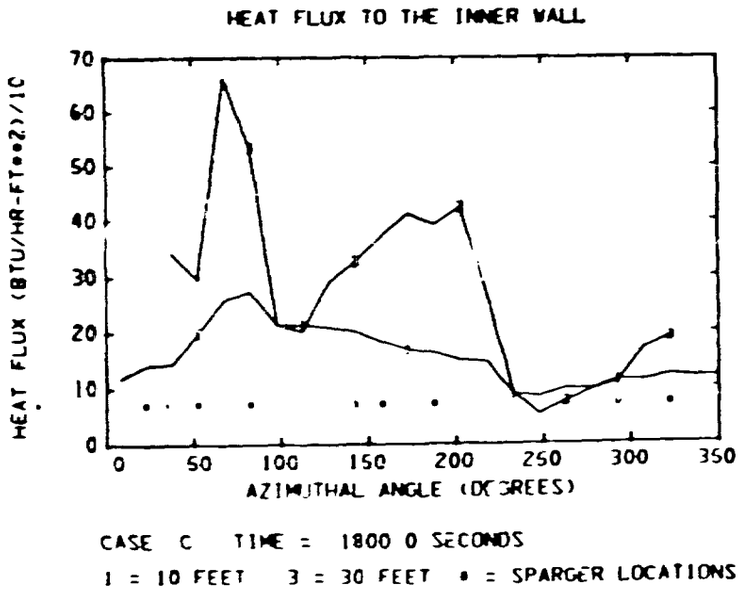

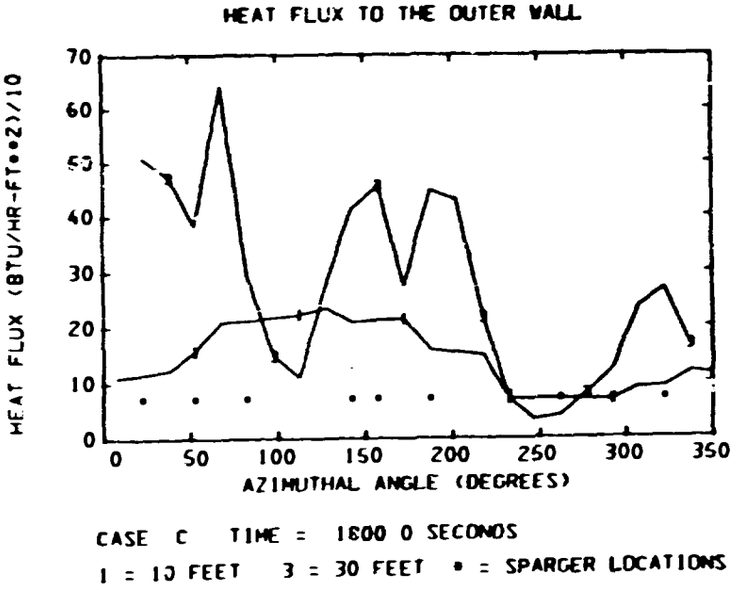

Fig. 20(continued) Heat flux to the Wet=Well Walls as a function of Azimuthal Position at Selected Times (600s top and 1800s bottom).

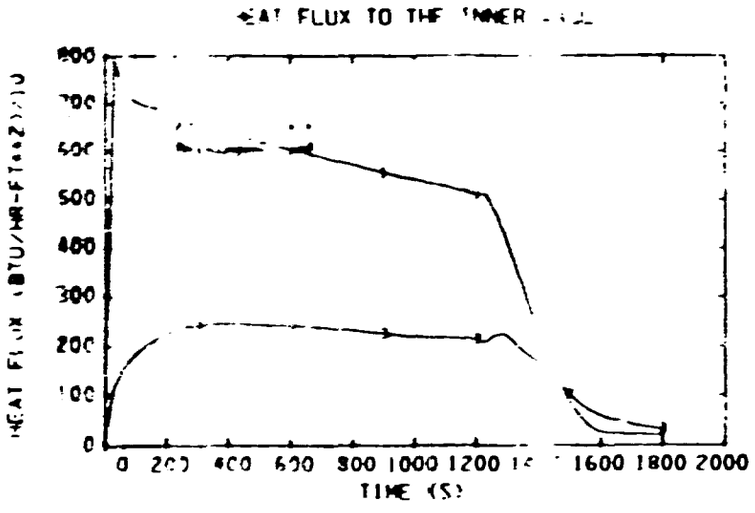

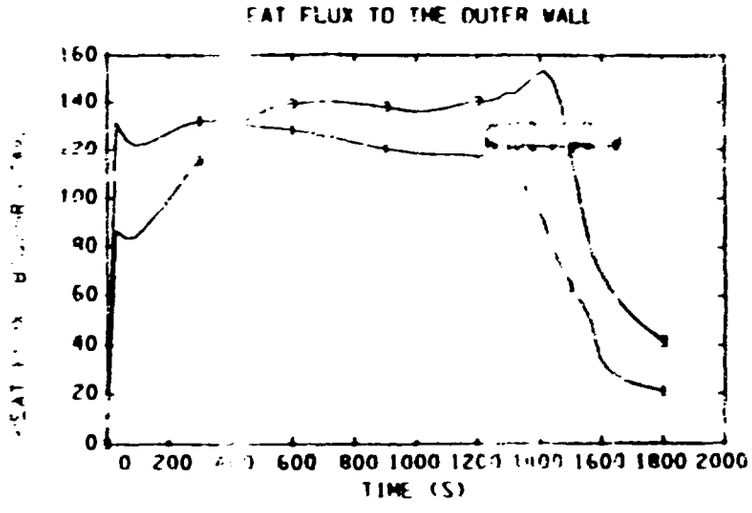

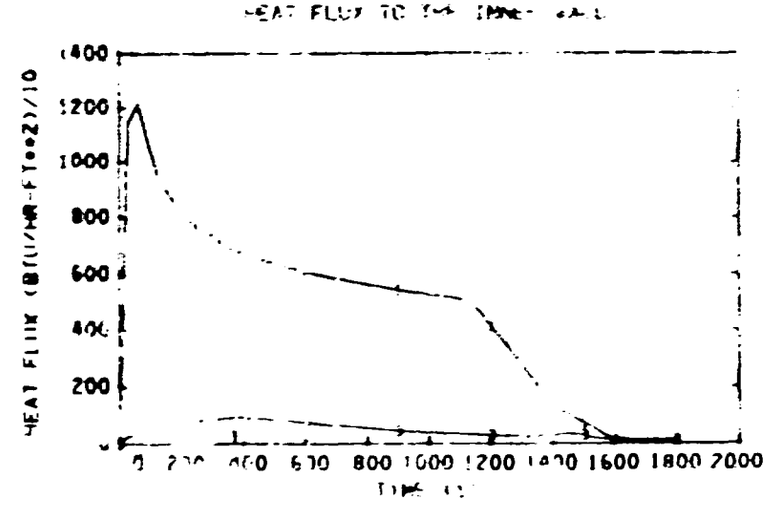

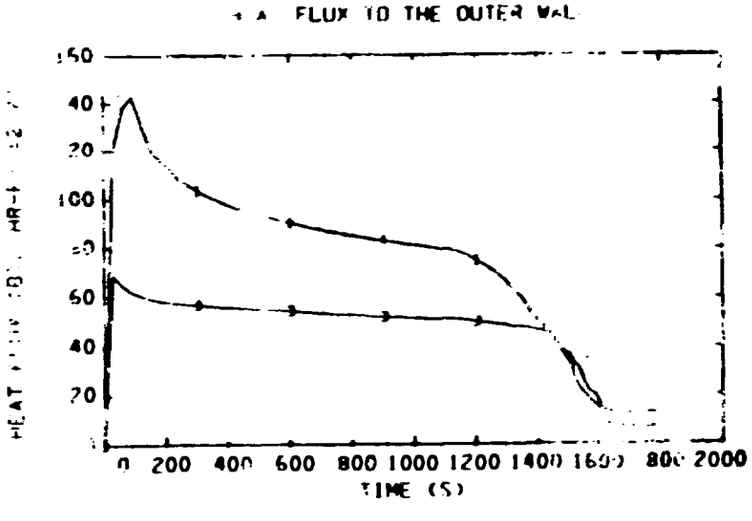

Heat Flux to the Wet-Wall Walls as a Function of Time at Selected Azimuthal Positions (142.5 and 292.5 Degrees).